Journal of Materials Chemistry C

Protonic conductivity in metalloprotein nanowires

Journal:	*Journal of Materials Chemistry C*
Manuscript ID	TC-ART-12-2022-005373.R1
Article Type:	Paper
Date Submitted by the Author:	13-Feb-2023
Complete List of Authors:	Lee, Woo-Kyung; US Naval Research Laboratory, Former Employee Bazargan, Gloria; US Naval Research Laboratory, Chemistry Division Gunlycke, Lennart; US Naval Research Laboratory, Chemistry Division Lam, Nga; University of New South Wales, School of Biotechnology and Biomolecular Sciences Travaglini, Lorenzo; University of New South Wales, School of Biotechnology and Biomolecular Sciences Glover, Dominic; University of New South Wales, School of Biotechnology and Biomolecular Sciences Mulvaney, Shawn; US Naval Research Laboratory, Former Employee

Protonic conductivity in metalloprotein nanowires

Woo-Kyung Lee,[1] Gloria Bazargan,[2*] Daniel Gunlycke,[2] Nga T. Lam,[3] Lorenzo Travaglini,[3] Dominic J. Glover,[3] and Shawn P. Mulvaney[1]

[1]*Former Employee, U.S. Naval Research Laboratory, Washington, DC, 20375 USA*

[2]*Chemistry Division, U.S. Naval Research Laboratory, Washington, DC, 20375 USA*

[3]*School of Biotechnology and Biomolecular Sciences, University of New South Wales, Sydney, NSW, 2052, Australia*

ABSTRACT

The development and processing of materials for devices that meaningfully translate signals between biology and electronics is a major challenge in materials science. Protonics-based devices are analogous to electronic devices but use protons as charge carriers instead of electrons. These devices show promise for interfacing with biological systems that commonly employ protons to perform work and transmit information. Proton-conductive materials (PCMs), the media through which protons are transported in protonic devices, are a key target for development because PCMs dominate the performance of these devices. We investigate protonic devices with a bundle of electrically conductive metalloprotein nanowires (MPNs) and palladium hydride (PdH_x) protodes, the proton-injecting contact, to analyze how proton transport depends on the chemical groups in proteins. Current–voltage (I–V) measurements of the protonic devices under hydrogen atmospheres show that the MPN bundles exhibit high protonic conductivity, enhancing the device conductivity by a factor of 4-5 when compared to an environment without hydrogen. First-principles-based molecular dynamics simulations suggest that the high concentration of carboxylic acid groups in the protein nanowires contributes to their protonic conductivity.

*Corresponding author
E-mail address: gloria.bazargan@nrl.navy.mil

Introduction

Establishing communication between biotic and abiotic systems is a major challenge in the development of biocompatible devices. This is because biological environments rely on small molecules and ions for signaling,[1-3] while traditional semiconductors depend on electronic movement. Recent efforts to address this challenge have focused on the emerging class of protonic devices[4, 5] that can deliver a controlled flow of protons to biological systems. Protonic devices

contain a proton (H^+) source and a "protode," most often palladium hydride (PdH_x), that releases protons via the electrochemical hydrogen oxidation reaction (HOR).[6] These protons then flow through a proton-conductive material (PCM) that is in direct contact with a biological medium. As protonic devices rely on PCMs to facilitate protonic movement, developing materials that are suitable for device integration can aid in the advancement of biocompatible technologies, *e.g.,* next-generation prosthetics and wound-healing therapies.[7]

Owing to their intrinsic biocompatibility, protein-based materials are promising candidates for interfacing with biological systems. Protein materials are structurally diverse, tunable through physical or chemical modification, and can be produced at large scales through well-established procedures.[8] Long-range proton transfer has been reported in several protein materials, including thin films based on reflectin[9] and membranes made up of supercharged polypeptides.[10] Proton conduction in these assemblies has been attributed to high concentrations of carboxylic-acid-containing moieties, which increase the number of available proton transfer pathways when hydrated. Similarly, chemical functionalization with carboxylic acid groups in metal-organic frameworks[11] and carboxymethyl groups in cellulose[12] is reported to increase the protonic conductivity of those materials. Advances in protein structure prediction and design have enabled the creation of protein assemblies with specific structural dimensions and functional properties.[13] Recent examples of protein engineering have demonstrated the fabrication of electrically conductive nanowires by aligning metalloproteins along a filamentous protein backbone to enable long-range electron transfer.[14, 15] In a similar manner, metalloprotein nanowires that are rich in carboxylic-acid containing residues could potentially be conductive to protons in addition to electrons.

The creation of PCM protein nanowires that efficiently transfer ionic and electronic signals have potential application in materials that seek to communicate signals and information between physical devices and biological functionalities, including enzymes and living cells. Herein we report the fabrication of protonic devices containing metalloprotein nanowires (MPNs). Electrically conductive metalloprotein nanowires were previously fabricated by decorating an ultrastable filamentous protein called gamma-prefoldin (γPFD) with tetra-heme cytochrome c3 proteins.[15] The γPFD subunits were conjugated to cytochrome c3 (cytc3) using SpyTag/SpyCatcher chemistry, with the C-terminus of the γPFD and cytc3 proteins genetically fused to a SpyTag or SpyCatcher domain, respectively, as shown in Figure 1a. The cytc3-labeled

γPFD filaments were shown to be capable of long-range electron transfer by electrochemical measurements of the MPNs conducting current between electrodes at the redox potential of cytc3. The γPFD-cytc3 MPNs may also be capable of mediating proton conduction as the γPFD subunits are rich in carboxylic acid groups. In particular, the helical regions of γPFD are composed of 22% aspartic and glutamic acid residues, which likely provide a sufficient density of carboxyl groups for the exchanging of protons along the nanowire shown in Figure 1b.

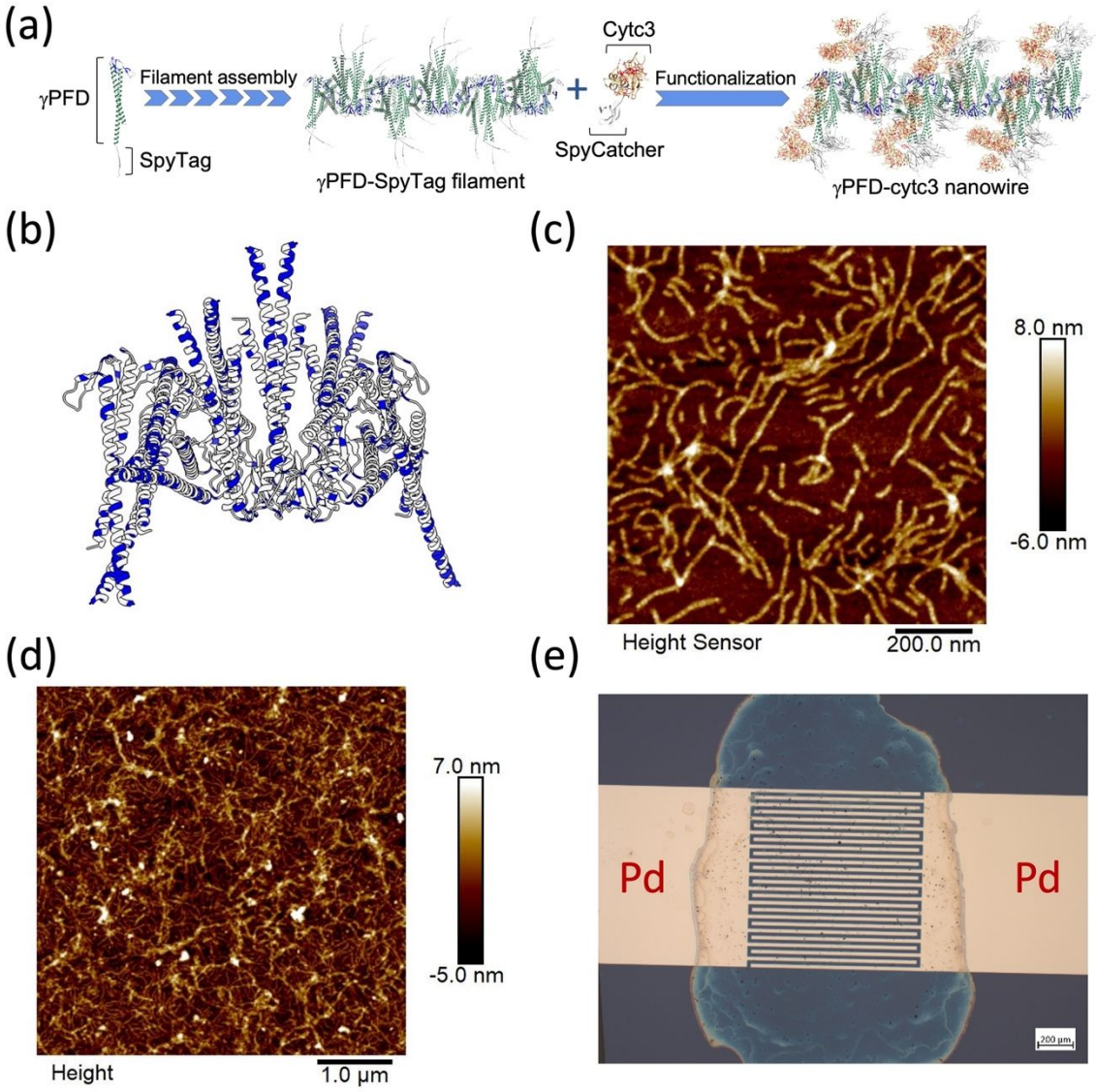

Fig. 1 Design and fabrication of metalloprotein nanowires (MPNs) for proton transfer. (a) Self-assembly of γPFD-SpyTag filaments and conjugation of cytc3-SpyCatcher and γPFD-SpyTag into γPFD-cytc3 MPNs. (b) The γPFD filament subunits are rich in carboxylic acid-containing residues as highlighted in blue. Atomic force microscope (AFM) images of (c) individual MPNs at low concentration (0.5 μM) and (d) the formation of a MPN film when deposited at a high

concentration (2 μM) on mica. (e) A microscope image of a high concentration of MPNs (2.5 μM) drop-casted protonic device.

We measured the current-voltage (I-V) characteristics of the fabricated protonic devices under hydrogen atmospheres. Our measurements show that the MPN bundles enhance protonic current in the device by a factor of ~4-5 when compared to an environment without hydrogen. We then carried out *ab initio* molecular dynamics (AIMD) simulations of carboxylic-acid-functionalized hydrocarbon wires to understand the role of these acid groups in facilitating protonic movement. Our simulations show that proton transfer through carboxylic acid groups enables movement over longer distances compared to Grotthuss hopping between water molecules, suggesting that the high concentration of acid groups in the MPNs contributes to their measured protonic conductivity. Overall, these results are the first demonstration of efficient protonic conductivity in engineered metalloprotein nanowires that are promising candidates for protonic devices.

Experimental

Protonic device fabrication

Photolithography was used to define the metal protodes used for electrical measurements of the protein nanowires. The protodes consisted of a 5 nm Ti sticking layer and 45 nm Pd metal layer that were deposited onto a 100 nm SiO_2/Si substrate. After metal patterning and liftoff, the substrate was cleaned by sonication in acetone and dried with the stream of N_2 gas. The MPNs were then deposited onto the metallized substrates.

Recombinant proteins expression and purification

The production of recombinant proteins was performed as described previously.[15] Briefly, the BL21 T7 Express strain of *E. coli* that contains plasmids encoding γPFD-SpyTag was grown in Luria Broth media with 100 μg mL^{-1} ampicillin at 37 ^{o}C. The expression of γPFD-SpyTag was induced with an addition of isopropylthiogalactoside (IPTG) to a final concentration of 0.4 mM and incubated for 16 h at 25 ^{o}C. The cell pellet was harvested and lysed in PBS buffer (20 mM sodium phosphate, 150 mM NaCl, pH 7.4) by sonication and γPFD-SpyTag filaments were purified using Capto™ Core 700 resin. Eluted fractions that contain pure protein were concentrated using 10 kDa Amicon Ultra-15 centrifugal filters (Merck), followed by lyophilization and storage at −80 °C. For expression of metalloproteins, an *E. coli* strain that contains both cytc3-

SpyCatcher and pEC86 plasmids was grown in grown at 37 °C in 2xYT media containing 100 μg mL^{-1} ampicillin and 34 μg mL^{-1} of chloramphenicol. Protein expression was induced addition of IPTG to a final concentration of 30 μM and incubated for 16 h at 25 ^{o}C. The cytc3-SpyCatcher was purified from periplasmic fractions using cation exchange chromatography by a HiTrap SP Sepharose FF column (GE Healthcare). Fractions containing the pure cytc3-SpyCatcher protein were concentrated, and buffer exchanged to PBS buffer, following by lyophilization and storage at −80 °C.

Assembly of metalloprotein nanowires and buffer exchange

Lyophilized γPFD-SpyTag and cytc3-SpyCatcher proteins were separately resuspended in PBS at pH 7.4 and incubated overnight at 4 ^{o}C to enable protein refolding. Covalent conjugation of cytc3 and γPFD-SpyTag filaments was achieved by combining an equimolar ratio of cytc3- SpyCatcher with γPFD-SpyTag. Subsequently, the assembled MPNs were buffer exchanged into milli-Q water using 2 kDa molecular weight cut-off Slide-A-Lyzer MINI dialysis devices and stored at 4 ^{o}C.

Atomic force microscopy of MPNs

The filamentous structure of MPNs was characterized by atomic force microscopy (AFM) on a mica substrate. A mica disc (12 mm in diameter, grade V-1 Ruby Muscovite-Bruker) was mounted on a specimen metal disc (Ted Pella Inc.) with an STKYDOT adhesive pad (Bruker). Fresh mica surfaces were produced by peeling off the top mica layer three times with adhesive tapes. Subsequently, 10 μL of MPNs in PBS (0.5 μM) was deposited and incubated on the fresh mica substrate for 2 min. The sample was rinsed with milli-Q water using a transfer pipet and the excess water was absorbed with Kimwipes. AFM was performed using an 8 nm tip radius probe (FMV-A, Bruker) with a nominal spring constant of 2.8 N/m and resonance frequencies of 75 kHz. The specimen was loaded onto a MultiMode 8-HR (Bruker) magnetic sample holder and imaged using Peakforce tapping technique with ScanAsyst-Air mode for self-optimizing AFM scan parameters. The AFM images of protein nanowires were operated with 256 pixels per line of resolution, scan rate of 0.5 Hz and dimension of 5 μm square. Images was processed using the NanoScope Software (Bruker).

Characterization of electrical and protonic conductivity

A probe station with custom-built environmental controlled chamber and Keithley 4200 semiconductor analyzer was used to characterize electrical property of protonic devices. The resistance of devices was characterized by a two-point probe measurement between Pd (or Au for control) electrodes under controlled relative humidity ranging from room humidity to 75% RH without H_2, and with 10% H_2 atmosphere. The relative humidity was controlled by bubbling nitrogen gas (no H_2) or 10%H_2/90% N_2 gas. Before each measurement, the RH inside chamber was stabilized at the target RH to be reached and was controlled by changing gas flow into the bubbler.

***Ab initio* molecular dynamics (AIMD) simulations**

We prepared periodic structural models of COOH-functionalized hydrocarbon wires at four degrees of functionalization: 25, 50, 75, and 100%, enforcing an overall density of 1 g cm^{-3}. Each simulation cell contains four main-chain carbon atoms, 8 water molecules, and one excess proton. These models allow us to examine the mechanisms of proton transfer involving carboxylic acid groups. All systems were simulated in the canonical NVT ensemble at 300 and 400 K. Following 30 picoseconds of equilibration, fifty 20-ps production trajectories were computed for each level of acid functionalization. The canonical sampling through velocity rescaling (CSVR) thermostat[16] was used to control the temperature. Time constants of 1 and 1,000 fs were used for equilibration and production runs, respectively. The electronic structure was described using the Gaussian and Plane Waves (GPW) method with the revPBE exchange-correlation functional,[17] GTH pseudopotentials,[18] TZV2P basis set, and Grimme's D-3 dispersion correction.[19] Cutoff energies of 300 and 30 Ry were used for the plane-waves and real-space grid, respectively. All *ab initio* molecular dynamics (AIMD) simulations were performed using the Quickstep module[20,21] within CP2K.[22]

The excess H^+ was tracked according to the scheme of Fischer and colleagues.[23] Initially, each hydrogen is assigned to its nearest heavy atom, and the water molecule with three assigned hydrogen atoms is identified as the hydronium (H_3O^+) ion. At each subsequent time-point, the position of the excess proton is defined based on the position of the H_3O^+ oxygen atom, and a change in this oxygen atom's identity is only counted if the excess H^+ at a given time-point *is not* one of the hydrogens that defined the previous logged H_3O^+ ion. This tracking scheme allows us to follow the movement of the excess H^+ while only counting true transfer events, rather than hops

that arise from the vibrational dynamics of proton rattling[24] between electronegative oxygen atoms. Further details about this proton tracking procedure are described in Ref. 23.

Results and Discussion

Assembled γPFD-cytoc3 MPNs were produced as previously described,[15] and bundles of diluted MPNs were deposited on mica and imaged by AFM (Fig. 1c). The average length and width of the individual MPNs were 1018 ± 253 nm and 3.89 ± 0.93 nm (n = 100 filaments), respectively, as determined from AFM images. The MPNs were shown at higher concentrations (≥ 2 μM) to form a crosslinked film on the mica (Fig. 1d). To measure proton conductance of MPNs, a concentrated of MPN solution (2.5 μM) was drop-casted on pre-fabricated Pd interdigitated electrodes (IDEs), which form PdH_x protodes under H_2-containing atmospheres (Fig. 1e). The Pd IDE contains 13 electrodes on each side that are 950 μm long and 20 μm wide, equally separated by a gap of 20 μm to maximize possible contacts with the bundles. Before drop casting the MPN solution, the protein solution was dialyzed against distilled water overnight at 4°C to remove NaCl residues to prevent the formation of NaCl crystals on the IDEs when drying. Failure to prevent NaCl crystal formation was shown to cause the electrical current to dominate the device conductance under RH higher than approximately 55% with hydrogen gas, presumably due to electrical conductivity through solvated NaCl crystals. Additional details are reported in the Supplementary Information.

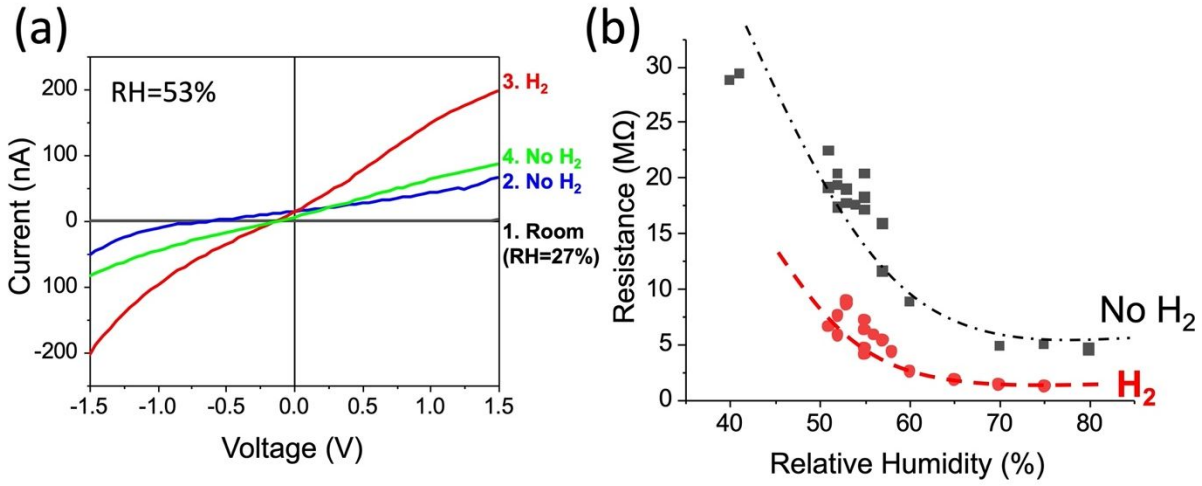

Fig. 2 (a) Typical current-voltage characteristics of our measurements with drop-casted MPNs on Pd-IDE with or without hydrogen gas under a relative humidity of 53%. The measurements were conducted sequentially under (1) ambient condition at RH=27%, (2) controlled RH=53% without hydrogen, (3) 10% hydrogen gas in N_2 at RH=53%, and (4) after purged with dry N_2 then controlled RH=53% without H_2 to test a reversible behavior. (b) The resistance of MPNs

on IDE without hydrogen (black) and with hydrogen gas (red) in the range of RH from 40% to 80%. Dotted lines are included for visual clarity only.

The conductivity of the MPNs deposited Pd IDE devices in a humidified (53% RH) nitrogen ambient environment was measured, both with and without hydrogen (H_2, 10% fraction) as shown in Figure 2a. Under 10% H_2 (red curve, #3), the current response in the I–V curves is 4-fold higher (~± 200 nA at ± 1.5 V) than that measured under humidified N_2 alone (~± 50 nA at ± 1.5 V, blue curve, #2). We typically measured I-V curves subsequently at room RH: (1) humidified N_2 alone, (2) humidified H_2/N_2, (3) and then completed the measurement with humidified N_2 alone, and (4) again to monitor its reversibility. Notably, we found that a dialysis of the MPNs' buffer solution before deposition on the Pd IDE is crucial to observe protonic currents. Without dialysis, NaCl was crystalized when drying and spanned over the Pd IDEs. As a result, electrical current from the solvated NaCl crystals screens the protonic currents above RH≈55%. Additional details are reported in the Supplementary Information.

Figure 2b shows that the dependence of the resistance of MPNs under controlled RH ranges from 40 to 80%. The resistance was estimated from I-V curves without hydrogen (black) and with 10% H_2 gas (red). The graph clearly shows a decrease in device resistance under H_2 gas (red) over the entire range of measured RH due to protonic currents. The resistance is approximately 4-5-fold lower than that measured without H_2 (black). Proton transport through MPNs could therefore be transduced to electrical conductivity of IDEs to decrease device resistance under the hydrogen atmosphere.

For control experiments, we prepared a gold IDE drop-casted with MPNs as shown in Figure 3a. The results of our measurements reported in Figure 3b show that there is no contribution from proton conduction under hydrogen gas. This indicates that Au electrodes are not able to transfer protons and that hydrogen uptake into Pd to form PdH_x is therefore crucial for these protonic devices.

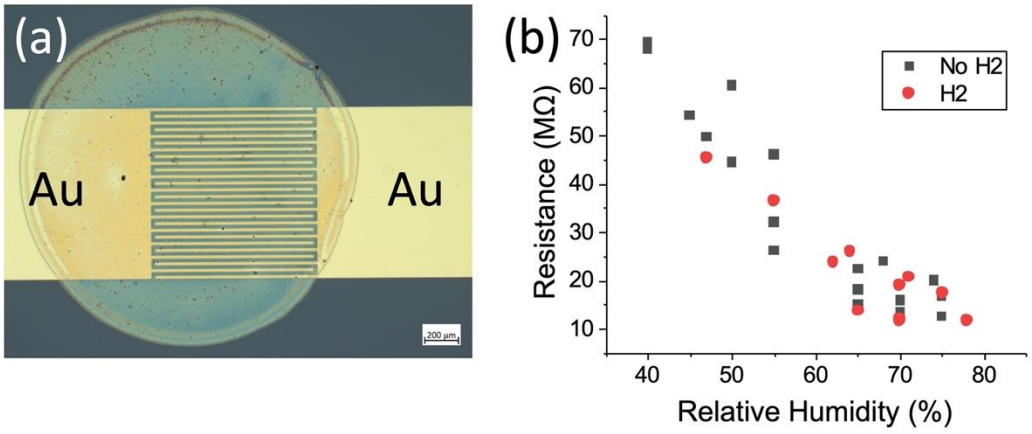

Fig. 3 (a) A gold IDE drop-casted with MPNs. (b) The resistance of gold IDEs drop-casted MPNs measured under controlled relative humidity ranging from 40 to 80% without (black) and with hydrogen gas (red).

To investigate the possible mechanism of proton conduction in protein nanowires we individually tested I-V characteristics of each MPN component – cytc3-SpyCatcher and γPFD-SpyTag – after dialysis of the proteins into distilled water. The heme containing cytc3-SpyCatcher exhibited relatively higher electrical conductivity in the entire range of RH as shown in Figure 4a. However, there was no significant change in the resistance of cytc3-SpyCatcher under H_2, indicating the component contributes only electrical conduction. Figure 4b shows that unlike cytc3-SpyCatcher, a slight decrease of resistance of filamentous γPFD-SpyTag under H_2 over the considered range of RH. The protonic conductance lowers the device resistance approximately 2-fold under hydrogen. Presumably, the acids groups in filament backbone also play an important role in proton conduction, as we observed in MPNs.[5]

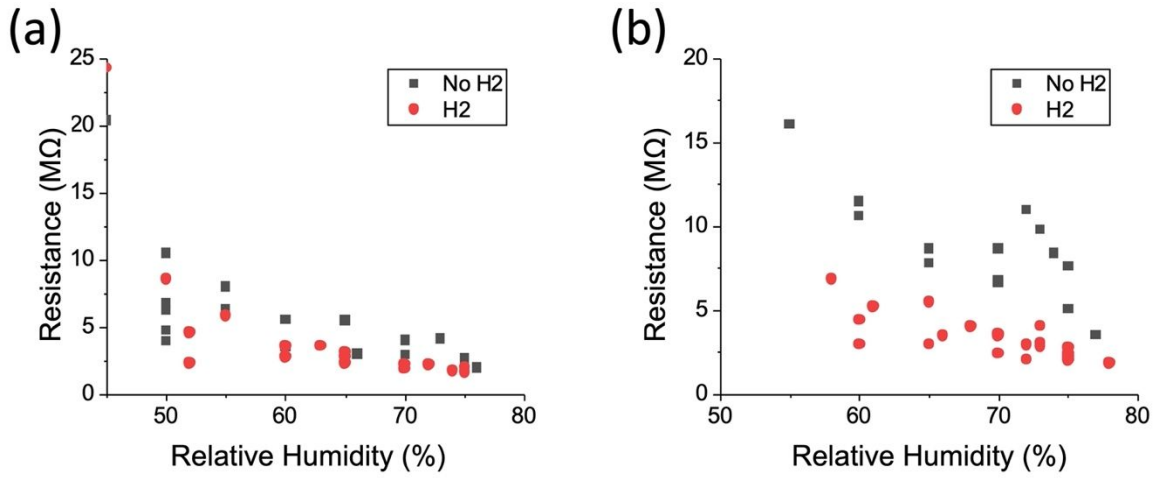

Fig. 4 (a) The resistance of Pd IDE of drop-casted metalloprotein (cytc3-SpyCatcher) solution measured under the relative humidity ranged from 50 to 75%. (b) The resistance of Pd IDE of drop-casted filamentous scaffold (γPFD-SpyTag) solution measured under the relative humidity ranged from 50 to 75%.

A primary motivation for characterizing the protonic conductivity of MPNs was to determine if protons can be transported through acids moieties in nanowires because designing functional protein nanowires with specific chemical groups to enhance or reduce proton conduction is crucial for bioelectronic device applications. To gain insight into the possible mechanisms of proton transport in MPNs, we carried out AIMD simulations of carboxylic-acid-functionalized hydrocarbon wires to probe the pathways of proton transfer involving COOH groups.

From these AIMD simulations we have identified two mechanisms of proton transfer involving carboxylic acid groups that enable longer H^+ transfer distances than a Grotthuss hop between water molecules. Mechanism 1 shown in Figure 5, is a two-step process and entails proton transfer across a single acid group as outlined below.

Mechanism 1

$$\mathbf{H_3O}^+ + \mathrm{COOH} + \mathrm{H_2O} \rightarrow \mathrm{H_2O} + \mathbf{C(OH)_2}^+ + \mathrm{H_2O} \quad (1)$$

$$\mathrm{H_2O} + \mathbf{C(OH)_2}^+ + \mathrm{H_2O} \rightarrow \mathrm{H_2O} + \mathrm{COOH} + \mathbf{H_3O}^+ \quad (2)$$

$$\mathbf{H_3O}^+ + \mathrm{COOH} + \mathrm{H_2O} \rightarrow \mathrm{H_2O} + \mathrm{COOH} + \mathbf{H_3O}^+ \quad \text{Overall}$$

As illustrated in Figure 5, the excess proton is first transferred from a hydronium (H_3O^+) ion to the carbonyl oxygen (C=O) of the acid group, and then from the hydroxyl (OH) moiety of the acid group to another water molecule to form a new hydronium ion. Note that this mechanism *does not* involve intramolecular proton transfer between oxygen atoms of the carboxylic acid group. We observe transfer events via Mechanism 1 at all considered acid concentrations (25-100%) and temperatures (300 and 400 K).

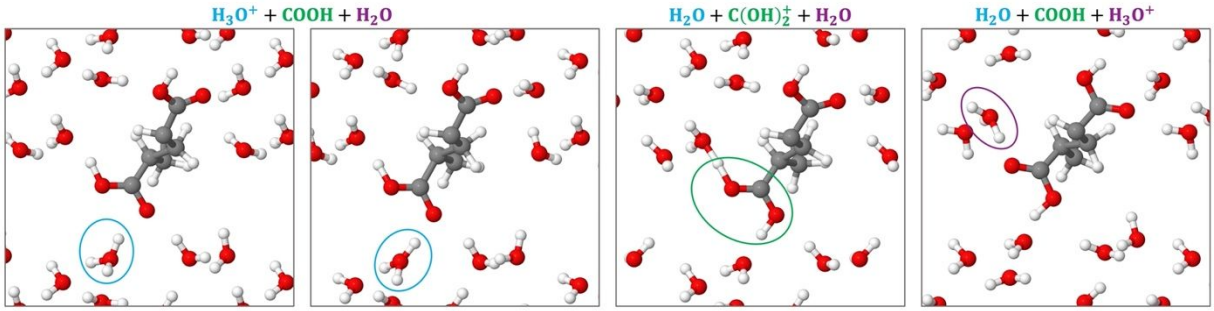

Fig. 5 Proton (H^+) transfer by Mechanism 1 across a single carboxylic acid group in the COOH-functionalized (50%) hydrocarbon wire at 400 K.

The second mechanism identified through our AIMD simulations is a multi-step process and entails proton transfer across *at least* two acid groups. The minimum reaction steps of Mechanism 2 are outlined below.

Mechanism 2

$$\mathbf{H_3O}^+ + COOH + COOH + H_2O \rightarrow H_2O + \mathbf{C(OH)_2}^+ + COOH + H_2O \quad (1)$$

$$H_2O + \mathbf{C(OH)_2}^+ + COOH + H_2O \rightarrow H_2O + COOH + \mathbf{C(OH)_2}^+ + H_2O \quad (2)$$

$$H_2O + COOH + \mathbf{C(OH)_2}^+ + H_2O \rightarrow H_2O + COOH + COOH + \mathbf{H_3O}^+ \quad (3)$$

$$\mathbf{H_3O}^+ + COOH + COOH + H_2O \rightarrow H_2O + COOH + COOH + \mathbf{H_3O}^+ \quad \text{Overall}$$

This mechanism involves: (1) proton transfer from a hydronium (H_3O^+) ion to the carbonyl oxygen

(C=O) of an acid group, (2) proton transfer from the hydroxyl of the acid group to another acid group, and (3) proton transfer from the hydroxyl of the second acid group to another water molecule to form a new hydronium ion. Note that step (2) can involve more than two acid groups, as shown in Figure 6, but a minimum of two is required. Because Mechanism 1 requires fewer distinct proton transfer steps and does not involve intramolecular proton transfer between COOH groups, our simulations predict that this type of transfer occurs more often than transfer by Mechanism 2.

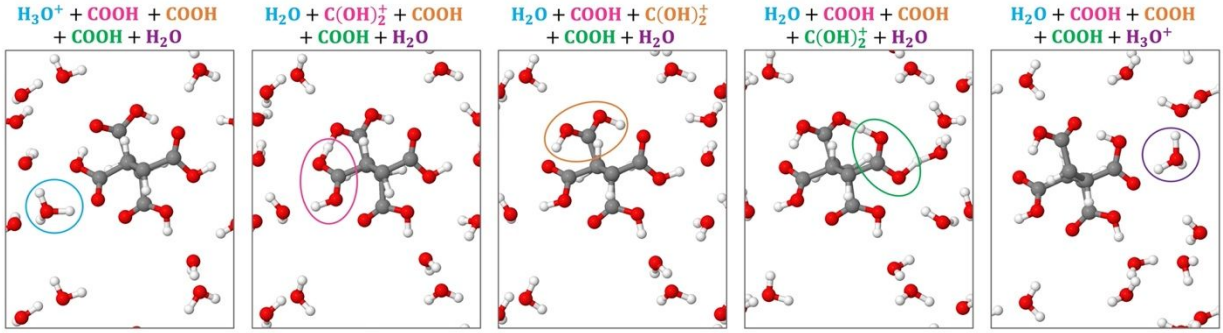

Fig. 6 Proton (H^+) transfer by Mechanism 2 across three carboxylic acid groups in the COOH-functionalized (100%) hydrocarbon wire at 400 K.

Similarly, an earlier study by Friedman and colleagues[25] used classical molecular dynamics simulations to examine proton transfer between carboxyl groups along the surface of the S6 ribosomal protein. Their results show that the carboxyl groups on the protein facilitate H^+ transfer through two pathways: (1) directly through carboxyl atoms only, and (2) as mediated by solvent, with intervening water molecules. For our model systems, Mechanism 2 as shown in Fig. 6, is a direct transfer pathway where a hydronium ion and a water molecule are the terminal proton donor and acceptor, respectively. A solvent-mediated proton transfer through a pathway that is similar to Mechanism 2 would likely occur in systems where the acid sites are more widely spaced and surrounded by water molecules. This would of course depend on the concentration and collective configuration of the involved proton hopping sites.

We then quantified the proton transfer distances in our predicted mechanisms to understand the efficiencies of these transfer events. The approximate H^+ transfer distances of Mechanism 1, Mechanism 2, and a Grotthuss hop between water molecules are compared in Table 1. Our

simulations predict that the excess H^+ travels approximately 2 Å during a Grotthuss hop between neighboring water molecules, 6 Å when transferred through a single COOH group via Mechanism 1, and 10 Å when transferred through three COOH groups via Mechanism 2. These results demonstrate that the carboxylic acid groups enable proton transfer over longer distances during individual transfer events compared to Grotthuss hopping between water molecules. It is therefore plausible that the high concentration of COOH groups in the metalloprotein nanowires contributes to their measured protonic conductivity.

Table 1: Approximate distances traveled by the excess proton r_{hop} when transferred through Grotthuss hopping, Mechanism 1 with one carboxylic acid group, and Mechanism 2 with three carboxylic acid groups.

Proton transfer mechanism	r_{hop}(Å)
Grotthuss hop between H_2O molecules	2
Mechanism 1 with one COOH group	6
Mechanism 2 with three COOH groups	10

Conclusions

Protonic devices containing metalloprotein nanowires as the proton-conductive material were fabricated and shown to conduct not only electrons, but also protons. Current–voltage measurements of these devices under hydrogen atmospheres show that the MPN bundles enhance the device conductivity by a factor of 4-5 when compared to an environment without hydrogen. The protons are transported through the carboxylic acid groups in the protein filament structure, suggesting that a higher acid density may further enhance conductivity. These results are the first demonstration of efficient protonic conductivity in engineered metalloprotein nanowires that are promising candidates for protonic devices. The protonic conductivity of the nanowire films may also enable the construction of devices that produce electrical currents by harvesting energy from ambient humidity. It has been shown previously that thick films of bacterial nanowires can generate continuous electric power in ambient environments.[26] It was suggested that ambient humidity generates a vertical gradient of H^+ ions in the bacterial nanowires with surface carboxylic groups serving as a source of exchangeable protons. We hypothesize that sufficiently thick films

of the metalloprotein nanowires will also produce power from ambient humidity. Furthermore, the engineerable metalloprotein nanowires may serve as a model system to study charge transfer in protein-based energy harvesting materials as both the electronic and protonic conductivities should be modifiable. We demonstrated that protonic devices can be constructed using modular protein filaments, which are potentially applicable as scaffolds for the fabrication and production of biocompatible devices for implant applications. Furthermore, filaments of γPFD possess engineerable interfaces that have been exploited previously to build nanostructures and spatially align functional molecules,[27, 28] such as enzymes and nanoparticles. Harnessing the protonic conductivity of these malleable filaments could enable the fabrication of structured materials that transfer signals and information between biotic and abiotic systems for various applications including biosensors, protonic transistors, and fuel cells. Future investigations could explore the protonic conductivity of composite materials made up of metalloprotein nanowires and other biocompatible materials.

Conflicts of Interest

There are no conflicts of interest to declare.

Acknowledgements

This work has been supported by the Office of Naval Research through the U.S. Naval Research Laboratory. D.J.G. is supported by the Office of Naval Research Global (N62909-21-1-2019). G.B. acknowledges the National Research Council Research Associateship Programs.

References

1. M. Wikstrom, V. Sharma, V. R. Kaila, J. P. Hosler and G. Hummer, *Chemical reviews*, 2015, **115**, 2196-2221.
2. M. Capasso, T. E. DeCoursey and M. J. Dyer, *Trends in cell biology*, 2011, **21**, 20-28.
3. K. Takata, T. Matsuzaki and Y. Tajika, *Progress in histochemistry and cytochemistry*, 2004, **39**, 1-83.
4. Y. Deng, E. Josberger, J. Jin, A. F. Roudsari, B. A. Helms, C. Zhong, M. Anantram and M. Rolandi, *Scientific reports*, 2013, **3**, 1-9.
5. Z. Hemmatian, T. Miyake, Y. Deng, E. E. Josberger, S. Keene, R. Kautz, C. Zhong, J. Jin and M. Rolandi, *Journal of Materials Chemistry C*, 2015, **3**, 6407-6412.
6. J. Robinson, J. Pietron, B. Blue, F. Perkins, E. Josberger, Y. Deng and M. Rolandi, *Journal of Materials Chemistry C*, 2017, **5**, 11083-11091.

7. W.-K. Lee, J. J. Pietron, D. A. Kidwell, J. T. Robinson, C. L. McGann, P. E. Sheehan and S. P. Mulvaney, *Journal of Materials Chemistry C*, 2019, **7**, 10833-10840.
8. N. T. Lam, J. B. McCluskey and D. J. Glover, *ACS Applied Bio Materials*, 2022.
9. D. D. Ordinario, L. Phan, W. G. Walkup IV, J.-M. Jocson, E. Karshalev, N. Hüsken and A. A. Gorodetsky, *Nature chemistry*, 2014, **6**, 596-602.
10. C. Ma, J. Dong, M. Viviani, I. Tulini, N. Pontillo, S. Maity, Y. Zhou, W. H. Roos, K. Liu and A. Herrmann, *Science advances*, 2020, **6**, eabc0810.
11. H. Wu, F. Yang, X.-L. Lv, B. Wang, Y.-Z. Zhang, M.-J. Zhao and J.-R. Li, *Journal of Materials Chemistry A*, 2017, **5**, 14525-14529.
12. A. Samsudin, W. M. Khairul and M. Isa, *Journal of Non-crystalline solids*, 2012, **358**, 1104-1112.
13. N. T. Lam, J. B. McCluskey and D. J. Glover, *ACS Applied Bio Materials*, 2022, **5**, 4668-4686.
14. L. Altamura, C. Horvath, S. Rengaraj, A. Rongier, K. Elouarzaki, C. Gondran, A. L. Maçon, C. Vendrely, V. Bouchiat and M. Fontecave, *Nature chemistry*, 2017, **9**, 157-163.
15. Y. X. Chen, N. L. Ing, F. Wang, D. Xu, N. B. Sloan, N. T. Lam, D. L. Winter, E. H. Egelman, A. I. Hochbaum and D. S. Clark, *ACS nano*, 2020, **14**, 6559-6569.
16. G. Bussi, D. Donadio and M. Parrinello, *The Journal of chemical physics*, 2007, **126**, 014101.
17. Y. Zhang and W. Yang, *Physical Review Letters*, 1998, **80**, 890.
18. S. Goedecker, M. Teter and J. Hutter, *Physical Review B*, 1996, **54**, 1703.
19. S. Grimme, J. Antony, S. Ehrlich and H. Krieg, *The Journal of chemical physics*, 2010, **132**, 154104.
20. M. Krack and M. Parrinello, *High performance computing in chemistry*, 2004, **25**, 29-51.
21. J. VandeVondele, M. Krack, F. Mohamed, M. Parrinello, T. Chassaing and J. Hutter, *Computer Physics Communications*, 2005, **167**, 103-128.
22. T. D. Kühne, M. Iannuzzi, M. Del Ben, V. V. Rybkin, P. Seewald, F. Stein, T. Laino, R. Z. Khaliullin, O. Schütt and F. Schiffmann, *The Journal of Chemical Physics*, 2020, **152**, 194103.
23. S. A. Fischer, B. I. Dunlap and D. Gunlycke, *Chemical science*, 2018, **9**, 7126-7132.
24. A. Chandra, M. E. Tuckerman and D. Marx, *Physical review letters*, 2007, **99**, 145901.
25. R. Friedman, E. Nachliel and M. Gutman, *Biochimica et Biophysica Acta (BBA)-Bioenergetics*, 2005, **1710**, 67-77.
26. X. Liu, H. Gao, J. E. Ward, X. Liu, B. Yin, T. Fu, J. Chen, D. R. Lovley and J. Yao, *Nature*, 2020, **578**, 550-554.
27. S. Lim, G. A. Jung, D. J. Glover and D. S. Clark, *Small*, 2019, **15**, 1805558.
28. D. J. Glover, L. Giger, S. S. Kim, R. R. Naik and D. S. Clark, *Nature communications*, 2016, **7**, 1-9.